# Two-parameters residual-moveout analysis for wave-equation migration velocity analysis

*Biondo Biondi*

## ABSTRACT

The use of two-parameter RMO functions has the potential of improving the flatness of RMO-corrected gathers. The two RMO functions I propose add a second term to the conventional angle-domain RMO function. The proposed RMO functions achieve improved flatness when applied to two test CIGs that are representative of situations when either strong lateral velocity variations or anisotropy occur.

The use of two-parameter RMO functions could also improve the velocity gradients when applied within automatic MVA methods. My numerical experiments indicate that the RMO function that I defined by adding a term proportional to the fourth power of the tangent of the aperture angle should yield more accurate gradients than the one-parameter RMO function. This choice is also more robust with respect to the setting of processing parameters than the other two-parameter RMO function I introduce in the paper, which adds a term proportional to the absolute value of the sine of of the aperture angle

## INTRODUCTION

The measurement of the residual moveout (RMO) in migrated common image gathers (CIG) is an important component of any migration velocity analysis (MVA) method. The choice of a robust method for measuring RMO is particularly important if the MVA process is automatized to avoid explicit picking of RMO parameters from coherency spectra (Biondi, 2008, 2010; Zhang and Biondi, 2011). In Biondi (2011), I illustrate with a simple example some of the challenges that these methods may encounter when a one-parameter RMO analysis is employed in presence of strong lateral velocity variations. To address these concerns, in this report I introduce two possible choices of RMO functions defined by two parameters instead of one. Both choices add a term to the RMO function, in addition to the usual term that is proportional to the square of the tangent of the aperture angle.

The first choice of RMO function adds a term proportional to the fourth power of the tangent of the aperture angle, and thus I will dub it the "Taylor" RMO function. The second choice adds a term proportional to the absolute value of the sine of the normalized aperture angle. The angle is normalized to enable the sine to complete a full cycle between zero and the maximum aperture angle used for the analysis. This

choice is motivated by the fact that it is theoretically desirable to have the terms of the RMO function to be mutually orthogonal (Siliqi, 2009). The sine function is only approximately orthogonal to the square of the tangent, but it has the advantage of being extremely simple. I will dub this RMO function "Orthogonal".

I test the efficacy of the proposed RMO functions using two CIGs that were obtained by migrating two different synthetic data sets. The first CIG represents the challenges presented by strong lateral velocity variations. The data were modeled assuming a strong negative velocity anomaly above a flat reflector (Biondi, 2011). The second CIG represents the effects of anisotropy on RMO analysis. The data were modeled assuming a strongly anisotropic VTI medium ($\epsilon = 0.0975$ and $\delta = -0.11$) above a flat reflector, and migrated assuming an isotropic velocity (Biondi, 2005).

In the following section I introduce the new RMO functions and apply them to compute two-dimensional spectra measuring the stack power as a function of the moveout parameters. In the subsequent section I analyze the accuracy of the potential search direction that would be computed by evaluating the gradient of the stack power as a function of the RMO parameters, and compare the results with the results of a similar analysis when the conventional one-parameter RMO analysis is applied.

## TWO-PARAMETER RMO FUNCTIONS

Biondi and Symes (2004) introduced the following one-parameter RMO function for angle-domain CIG:

$$\Delta z = (1 - \rho) \tan^2 \gamma, \tag{1}$$

where $\gamma$ is the aperture angle and $\Delta z$ is the difference between the imaged depth at normal incidence ($\gamma = 0$) and the imaged depth at a given angle $\gamma$. For constant velocity errors in the half space above the reflector, the parameter $\rho$ has a direct physical interpretation. It is related to the ratio between the current migration slowness $s_{\text{mig}}$ and the true slowness $s$; that is, $\rho \approx s_{\text{mig}}/s$. However, in the following discussion this physical interpretation of $\rho$ is irrelevant, and it can be simply considered as a free parameter describing a family of RMO functions.

What I call the Taylor RMO function adds the next higher-order even term to equation 1 as follows

$$\Delta z_T = (1 - \rho) \tan^2 \gamma + (1 - \lambda_T) \tan^4 \gamma, \tag{2}$$

where $\lambda_T$ is the additional free parameter. As in equation 1, the RMO function is equally flat when $\rho = 1$ and $\lambda_T = 1$.

The second two-parameter RMO function that I introduce adds a sine function to equation 1 as follows

$$\Delta z_O = (1 - \rho) \tan^2 \gamma + (1 - \lambda_O) \, |\sin \bar{\gamma}|, \tag{3}$$

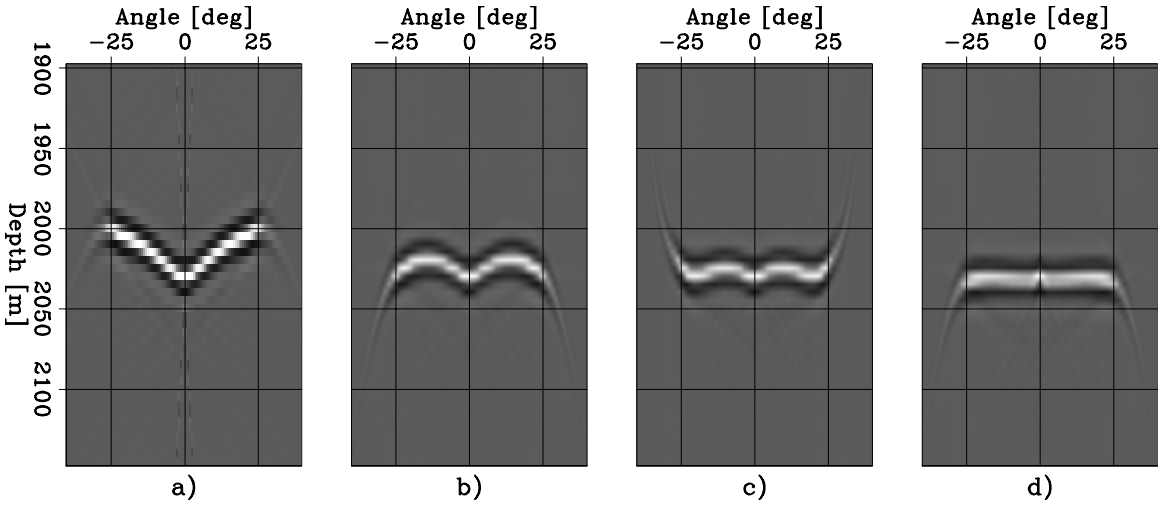


Figure 1: CIGs after constant velocity migration and: a) no correction, b) correction with a one-parameter RMO (equation 1), c) correction with the "Taylor" RMO (equation 2), and d) correction with the "Orthogonal" RMO (equation 3). [**CR**]

where $\lambda_O$ is the additional free parameter, $\bar{\gamma} = 2\pi\gamma/\gamma_{\max}$ is the normalized aperture angle, and $\gamma_{\max}$ is the maximum aperture angle used for the analysis.

Figure 1a shows the first CIG that I use for my study. It was obtained by migrating a synthetic data set that was modeled assuming a strong negative velocity anomaly above a flat reflector and migrated assuming a constant velocity (Biondi, 2011). This CIG is located under the center of the anomaly. Its moveout is not well described by the conventional RMO function expressed in equation 1 because the image at near angles is more affected by the anomaly than the image at far angles. Figure 1b shows the result of correcting this CIG using equation 1 with $\rho = 1.075$ that is the $\rho$ value corresponding to the maximum of the stack power picked from a stack-power spectrum. This corrected CIG is far from being flat.

Figure 2 shows stack-power spectra as a function of two parameters. The panel on the left (Figure 2a) was computed using the "Taylor" RMO function described by equation 2, whereas the panel on the right (Figure 2b) was computed using the "Orthogonal" RMO function described by equation 3. In both cases the stack power was computed over the range of $-25^o \leq \gamma \leq 25^o$. Consequently, I set $\gamma_{\max} = 25^o$ to compute the normalized angle $\bar{\gamma}$ in equation 3. The power spectra were averaged over a thick (200 m) depth interval and slightly smoothed along the RMO parameters $\rho$ and $\lambda$.

The maxima of both of these two-parameter spectra are not along the $\lambda = 1$ line, indicating that the two-parameter RMO improves the flatness with respect to the one-parameter RMO. Indeed, when the values corresponding to the maxima of the power spectra shown in Figure 2 are used to correct the original CIG I obtain flatter gathers than when using a one-parameter RMO. Figure 1c shows the result of

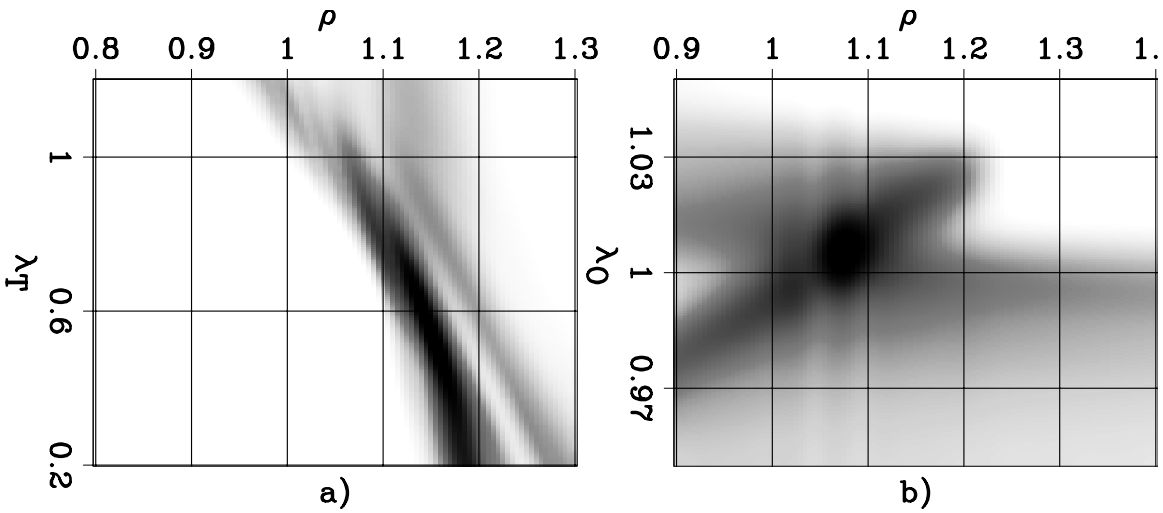


Figure 2: Two-parameter stack-power spectra resulting from RMO analysis of the migrated CIG shown in Figure 1a obtained applying: a) the "Taylor" RMO function (equation 2), and b) the "Orthogonal" RMO function (equation 3). [**CR**]

correcting the CIG shown Figure 1a using equation 2 with $\rho = 1.15$ and $\lambda_T = .55$. Figure 1c shows the result of correcting the CIG shown Figure 1a using equation 3 with $\rho = 1.075$ and $\lambda_O = 1.0055$. The CIG corrected using the "Orthogonal" RMO is almost perfectly flat within the $-25^o \leq \gamma \leq 25^o$ range.

Notice that the shape of the spectra around their respective maxima is substantially different between the two plots. The function corresponding to the "Orthogonal" RMO is more isotropic around the maximum than the one corresponding to the "Taylor" RMO. This behavior is expected because the two terms of the "Orthogonal" RMO function are close to be orthogonal with respect to each other. Theoretically, this more isotropic shape could lead to better gradients. However, we can also notice diagonal artifacts in Figure 2b. As we discuss below, the effects of these artifacts tend to outweigh any advantage provided by the more isotropic shape of the spectrum.

Figure 3a shows the second CIG that I use for my analysis. It was obtained by migrating a synthetic data set that was modeled assuming a strongly anisotropic VTI medium ($\epsilon = 0.0975$ and $\delta = -0.11$) above a flat reflector, and migrated assuming an isotropic velocity (Biondi, 2005). Because the anisotropy in the medium is not taken into account by the isotropic migration, the CIG moveout is not well described by the conventional one-parameter RMO function expressed in equation 1. Figure 1b shows the result of correcting this CIG using equation 1 with $\rho = .9375$ that is the $\rho$ value corresponding to the maximum of the stack power picked from a stack-power spectrum. This corrected CIG is far from being flat.

Figure 4 shows stack-power spectra as a function of two parameters. The panel on the left (Figure 4a) was computed using the "Taylor" RMO function described by equation 2, whereas the panel on the right (Figure 4b) was computed using the

"Orthogonal" RMO function described by equation 3. In both cases the stack power was computed over the range of $-50^o \leq \gamma \leq 50^o$. Consequently, I set $\gamma_{\max} = 50^o$ to compute the normalized angle $\bar{\gamma}$ in equation 3. The power spectra were averaged over a thick (200 m) depth interval and slightly smoothed along the RMO parameters $\rho$ and $\lambda$.

As for the spectra computed from the first CIG (Figure 2), the function corresponding to the "Orthogonal" RMO is more isotropic around the maximum than the one corresponding to the "Taylor" RMO. This difference in shape is less pronounced for this example than for the previous one.

Because the maxima of both of these two-parameter spectra are not along the $\lambda = 1$ line, we have indication that the two-parameter RMO improves the flatness with respect to the one-parameter RMO. Indeed, when the values corresponding to the maxima of the power spectra shown in Figure 4 are used to correct the original CIG I obtain flatter gathers than when using a one-parameter RMO. Figure 3c shows the result of correcting the CIG shown Figure 3a using equation 2 with $\rho = 0.915$ and $\lambda_T = 1.075$. Figure 3c shows the result of correcting the CIG shown Figure 3a using equation 3 with $\rho = 0.97$ and $\lambda_O = 0.988$. In particular, the CIG corrected using the "Taylor" RMO is significantly flatter, within the $-50^o \leq \gamma \leq 50^o$ range, than the one corrected using a one-parameter RMO.

## CONVERGENCE ANALYSIS

In the previous section I showed that we can obtain flatter migrated CIGs by applying a two-parameter RMO correction instead of a conventional one-parameter correction. These results would be sufficient to motivate the use of a two-parameter RMO if the goal were to improve the signal-to-noise in the stacked cube, or to perform velocity analysis by picking the stack-power maxima. However, I am interested in using the new RMO functions in an MVA method that avoids picking the maxima of coherency spectra; this method computes the gradients of the objective function from the gradient of the stack-power spectra with respective to the RMO parameters (Biondi, 2008, 2010; Zhang and Biondi, 2011). It is therefore important to analyze the quality of the gradient information computed from two-parameter spectra, and compare to the corresponding gradient information computed from one-parameter spectra.

As a quality measurements of the gradient information, I compute the correlation across the angle axis between the RMO function that would be computed by picking the maxima of the coherency spectra ${}_p\Delta z$ and the RMO function ${}_g\Delta z$ computed using the gradient.

For the "Taylor" RMO the reference RMO function ${}_p\Delta z_T$ is computed as follows:

$$ {}_p\Delta z_T\left(\gamma, \rho, \lambda_T\right) = \left(\rho - \widehat{\rho}\right) \tan^2 \gamma + \left(\lambda_T - \widehat{\lambda_T}\right) \tan^4 \gamma. \tag{4}$$

where $\left(\widehat{\rho}, \widehat{\lambda_T}\right)$ are the coordinates of the power-spectrum maximum. The RMO

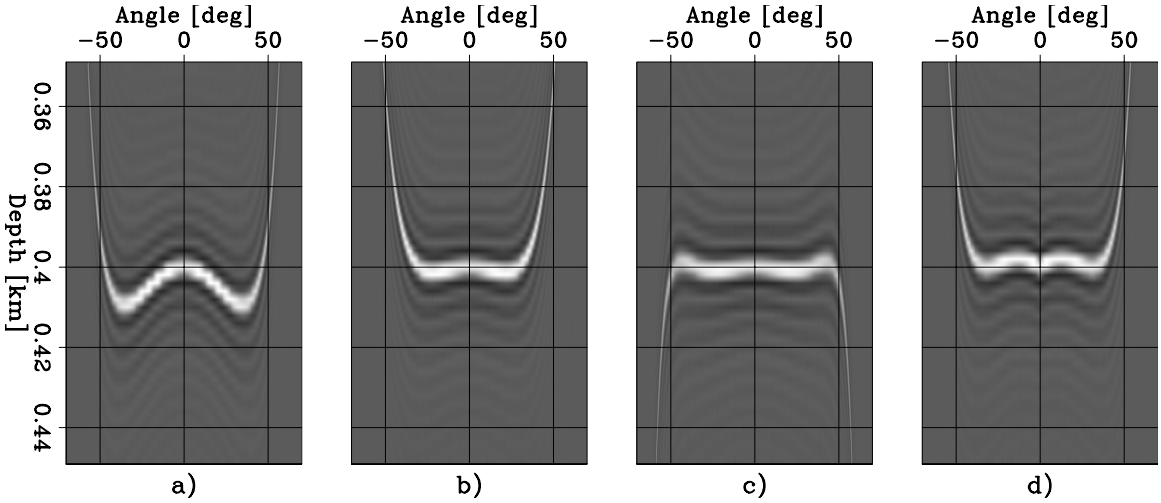


Figure 3: CIGs after isotropic velocity migration and: a) no correction, b) correction with a one-parameter RMO (equation 1), c) correction with the "Taylor" RMO (equation 2), and d) correction with the "Orthogonal" RMO shows the second CIG that I use (equation 3). [**CR**]

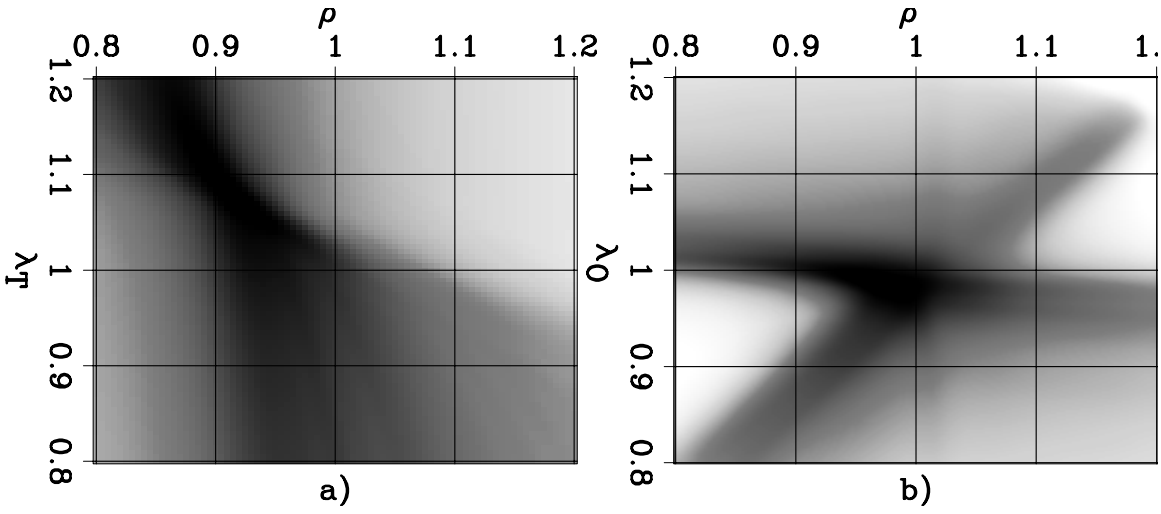


Figure 4: Two-parameter stack-power spectra resulting from RMO analysis of the migrated CIG shown in Figure 3a obtained applying: a) the "Taylor" RMO function (equation 2), and b) the "Orthogonal" RMO function (equation 3). [**CR**]

function ${}_g\Delta z_T$ computed from the gradient of the power spectrum $P_T$ is,

$$ {}_g\Delta z_T\left(\gamma,\rho,\lambda_T\right) = -\frac{\partial P_T}{\partial \rho}\left(\rho,\lambda_T\right)\tan^2\gamma - \frac{\partial P_T}{\partial \lambda_T}\left(\rho,\lambda_T\right)\tan^4\gamma, \tag{5}$$

and the correlation is computed as

$$ C_T\left(\rho,\lambda_T\right) = \sum_{\gamma} {}_p\Delta z_T\left(\gamma,\rho,\lambda_T\right)_g\Delta z_T\left(\gamma,\rho,\lambda_T\right). \tag{6}$$

I compare this correlation function over a range of $(\rho,\lambda_T)$ with the correlation function computed by

$$ C_{T1}\left(\rho,\lambda_T\right) = \sum_{\gamma} {}_p\Delta z_T\left(\gamma,\rho,\lambda_T\right)_g\Delta z_{T1}\left(\gamma,\rho,\lambda_T\right), \tag{7}$$

where the one-parameter RMO ${}_g\Delta z_{T1}$ is computed as follows

$$ {}_g\Delta z_{T1}\left(\gamma,\rho,\lambda_T\right) = -\frac{\partial P_T}{\partial \rho}\left(\rho,\lambda_T\right)\tan^2\gamma. \tag{8}$$

Figure 5 compares the correlation functions $C_T$ (panel a) and $C_{T1}$ (panel b) for the first CIG analyzed (Figure 1a). The asterisk superimposed onto the plots of the correlation functions is located at the maximum of the power spectrum displayed in Figure 2a. The coordinates $\left(\widehat{\rho},\widehat{\lambda_T}\right)$ of this maximum are used to evaluate the moveout ${}_p\Delta z_T$ according to equation 4. Accurate gradient directions correspond to positive correlation (plotted in white in the figure), whereas potentially misleading gradient directions correspond to negative correlation (plotted in black in the figure).

The correlation functions are mostly positive over a wide range of parameters $(\rho,\lambda_T)$, indicating that a velocity estimation method based on these RMO functions is likely to have good global convergence properties. In particular, the positive correlation functions at $(\rho=1,\lambda_T=1)$ indicates that the gradient computed starting from the migrated CIG shown in Figure 2a would be accurate, even if this CIG is far from being flat.

The correlation functions shown in Figure 5 are very similar. Therefore, the global convergence of the velocity estimation would be robust independently of whether the one-parameter or the two-parameter RMO function is used.

Similar correlation analysis of the RMO function can be performed when applying the "Orthogonal" RMO instead of the "Taylor" RMO. In this case the reference RMO function ${}_p\Delta z_O$ is computed as follows:

$$ {}_p\Delta z_O\left(\gamma,\rho,\lambda_O\right) = \left(\rho-\widehat{\rho}\right)\tan^2\gamma + \left(\lambda_O-\widehat{\lambda_O}\right)\left|\sin\bar{\gamma}\right|. \tag{9}$$

where $\left(\widehat{\rho},\widehat{\lambda_O}\right)$ are the coordinates of the corresponding power-spectrum maximum. The RMO function ${}_g\Delta z_O$ computed from the gradient of the power spectrum $P_O$ is,

$$ {}_g\Delta z_O\left(\gamma,\rho,\lambda_O\right) = -\frac{\partial P_O}{\partial \rho}\left(\rho,\lambda_O\right)\tan^2\gamma - \frac{\partial P_O}{\partial \lambda_T}\left(\rho,\lambda_O\right)\left|\sin\bar{\gamma}\right|, \tag{10}$$

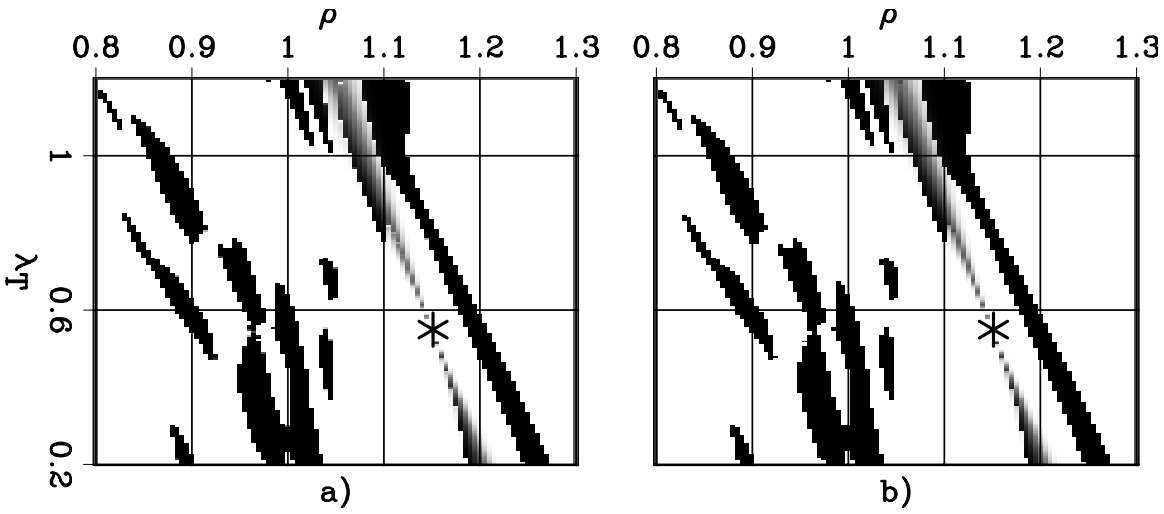


Figure 5: Correlation functions corresponding to the CIG shown in Figure 1a for: a) the "Taylor" two-parameter RMO function (equation 6), and b) the one-parameter RMO function (equation 7). [**CR**]

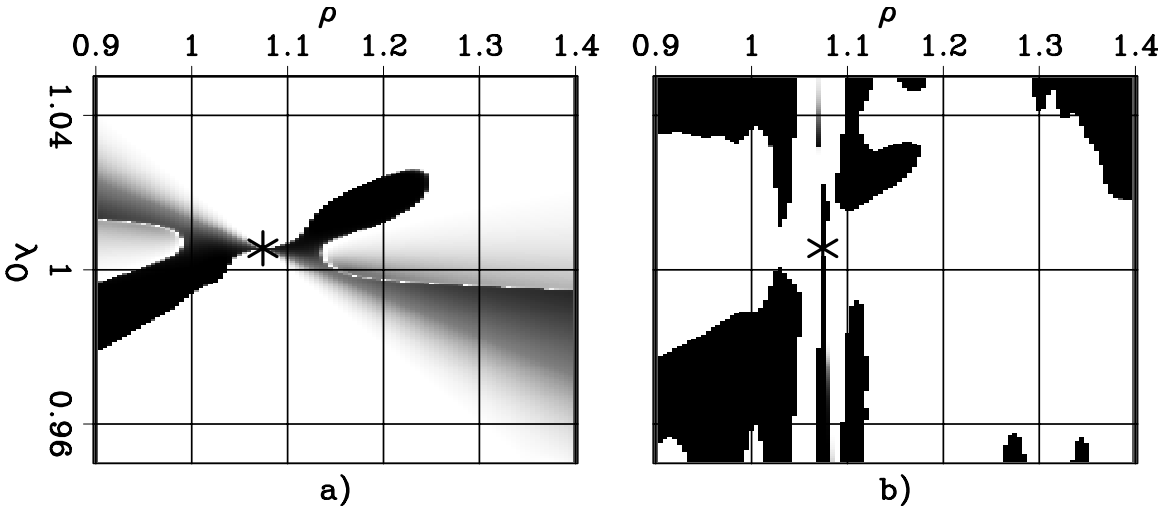


Figure 6: Correlation functions corresponding to the CIG shown in Figure 1a for: a) the "Orthogonal" two-parameter RMO function (equation 11), and b) the one-parameter RMO function (equation 12). [**CR**]

and the correlation is computed as

$$C_O\left(\rho,\lambda_O\right)=\sum_{\gamma}{}_p\Delta z_O\left(\gamma,\rho,\lambda_O\right){}_g\Delta z_O\left(\gamma,\rho,\lambda_O\right). \tag{11}$$

This correlation is compared with the correlation

$$C_{O1}\left(\rho,\lambda_O\right)=\sum_{\gamma}{}_p\Delta z_O\left(\gamma,\rho,\lambda_O\right){}_g\Delta z_{O1}\left(\gamma,\rho,\lambda_O\right), \tag{12}$$

where the one-parameter RMO ${}_g\Delta z_{O1}$ is computed as follows

$${}_g\Delta z_{O1}\left(\gamma,\rho,\lambda_O\right)=-\frac{\partial P_O}{\partial\rho}\left(\rho,\lambda_O\right)\tan^2\gamma. \tag{13}$$

Figure 6 compares the correlation functions $C_O$ (panel a) and $C_{O1}$ (panel b) for the first CIG analyzed (Figure 1a). The asterisk superimposed onto the plots of the correlation functions is located at the maximum of the power spectrum displayed in Figure 2b. The coordinates $\left(\widehat{\rho},\widehat{\lambda_O}\right)$ of this maximum are used to evaluate the moveout ${}_p\Delta z_O$ according to equation 9. As for the previous figure, accurate gradient directions correspond to positive correlation (plotted in white in the figure), whereas potentially misleading gradient directions correspond to negative correlation (plotted in black in the figure).

In this case the correlation functions shown in Figure 6 are not as similar as in the previous case. In particular, the black area around the value $(\rho=1,\lambda_O=1)$ in Figure 6a indicate that the two-parameter RMO analysis would provide unreliable gradients. This problem is related to the diagonal artifacts visible in the power spectrum shown in in Figure 2a. These artifacts are caused by the fact that the second term in the "Orthogonal" RMO function has an extremum in the middle of the angular range, in contrast with the other RMO functions that have an extremum at normal-incidence. This mid-range extremum causes spurious local maxima of the spectrum at depths different than the normal incidence depth of the imaged reflector. These artifacts are much weaker when I averaged the power spectrum over a thinner depth interval (30 m) than the one used for computing the function displayed in Figure 6a. The new averaging window is of thickness comparable to the image of the reflector. Figure 7a shows the power spectrum obtained with this thinner averaging window, and Figure 7b corresponds to the two-parameters correlation function, which is a substantial improvement with respect to the one shown in Figure 6a. Figure 8 and Figure 9 shows the analysis of the correlation functions for the second CIG analyzed (Figure 3a); that is, the CIG suffering from the effects of anisotropy. Figure 8 corresponds to the "Taylor" RMO function, whereas Figure 9 corresponds to the "Orthogonal" RMO function. For this CIG, the two-parameter RMO analysis seems to improve the global convergence of the method, in particular when the "Orthogonal" function is applied (Figure 9).

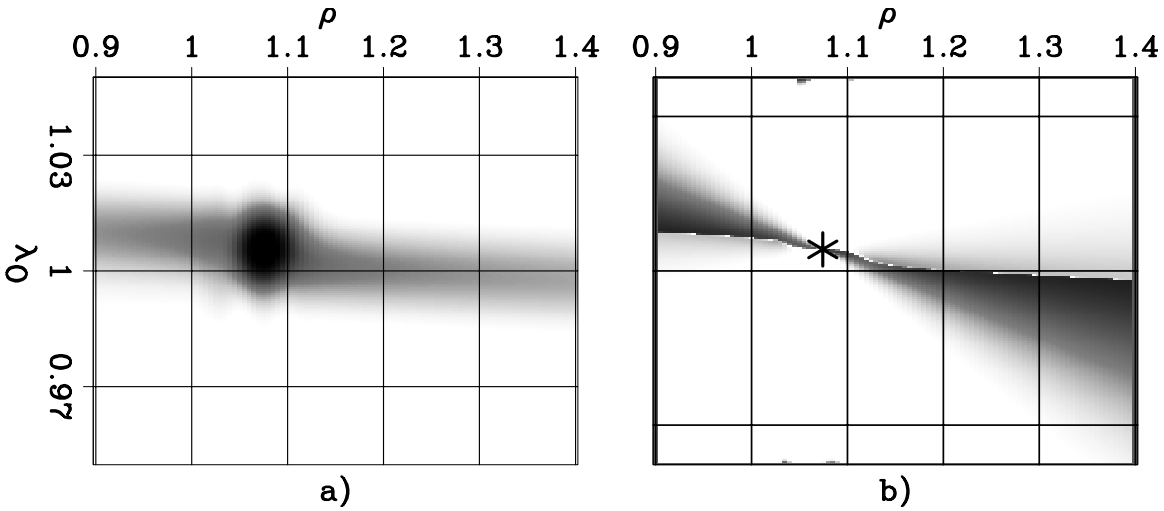


Figure 7: Panel a): Two-parameter stack-power spectra resulting from RMO analysis of the CIG shown in Figure 1a obtained using a thinner averaging window (30 m) than the one used to compute the spectrum shown in Figure 2b. Panel b): Correlation function for the "Orthogonal" two-parameter RMO function obtained using the thinner averaging window. [**CR**]

## Local convergence analysis

To gain an insight whether using a two-parameter RMO provides more accurate gradients starting from a CIG that is already close to be flat, we can zoom into the previous correlation plots around the location of the maximum. The correlation function in these smaller windows is related to "local convergence" of velocity estimation methods based on the selected RMO functions.

Figure 10 shows the zooms into the plots shown in Figure 5; that is, comparing the correlation function for the first CIG (velocity anomaly) obtained using the "Taylor" RMO function (Figure 10a) and the conventional one-parameter RMO function (Figure 10b). I set the width of the close up windows to be equal to the distance of the maximum from the starting CIG; that is, the difference between the minimum and the maximum value of the $\rho$ parameter is $\Delta\rho = (\widehat{\rho} - 1)$ and the difference between the minimum and the maximum value of the $\lambda_T$ parameter is $\Delta\lambda_T = \left(\widehat{\lambda_T} - 1\right)$. The two plots shown in Figure 10 are almost identical, indicating that in this case there would be a negligible advantage to be gained by employing a two-parameter RMO function.

Figure 11 analyze the application of the "Orthogonal" RMO function to the same CIG as the previous figure. It shows the zooms into the plots shown in Figure 7b and Figure 6b, respectively. I set the window width following the same criterion described above for the "Taylor" RMO function. In this case, the one-parameter RMO function seems to provide better local convergence than the two-parameter RMO function.

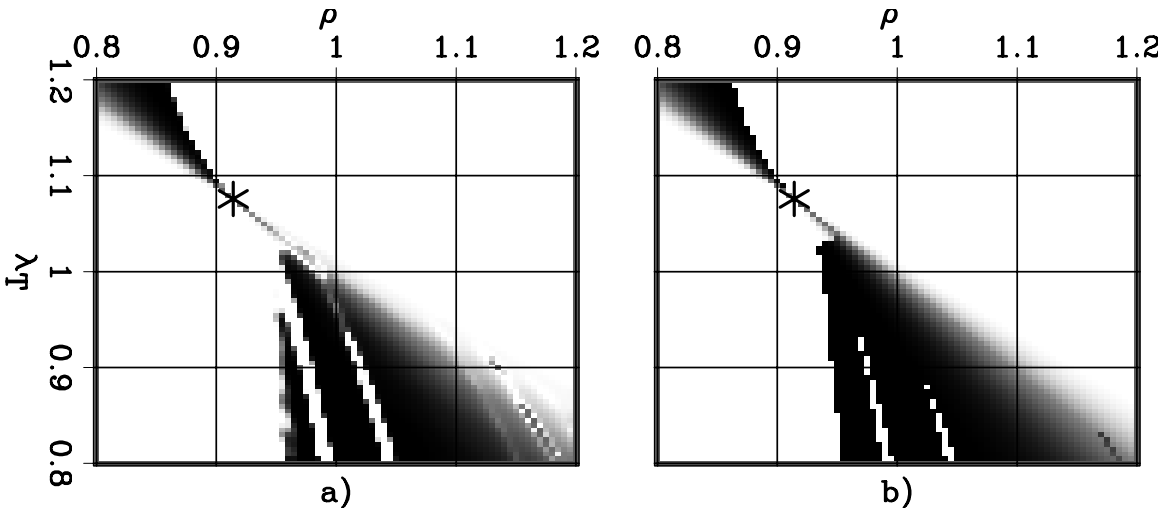


Figure 8: Correlation functions corresponding to the CIG shown in Figure 3a for: a) the "Taylor" two-parameter RMO function (equation 6), and b) the one-parameter RMO function (equation 7). [**CR**]

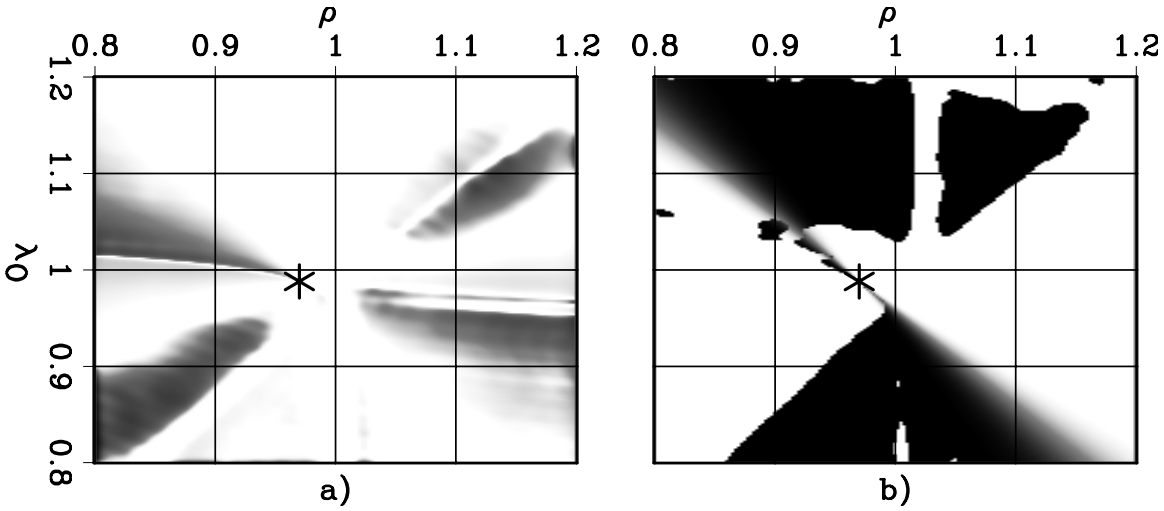


Figure 9: Correlation functions corresponding to the CIG shown in Figure 3a for: a) the "Orthogonal" two-parameter RMO function (equation 11), and b) the one-parameter RMO function (equation 12). [**CR**]

The last two figures, Figure 12 and Figure 13, show similar analysis as the previous two, but applied to the CIG that suffers from the effects of anisotropy. For these CIG the two-parameters RMO function provides a better local convergence than the one-parameter function. The improvements look more substantial for the "Orthogonal" RMO function than for the "Taylor" RMO function.

## DISCUSSION AND CONCLUSIONS

The introduction of a second term to the conventional RMO function for angle-domain CIGs improves the flatness of the corrected gathers for both CIGs I used in my testing and for both choices of two-parameter RMO function I proposed.

The answer to the question of whether using a two-parameter RMO function yields more reliable gradients when applied in automatic MVA methods is more ambiguous. The correlation analysis I presented indicates that the "Taylor" RMO function yields more robust gradients than the simple one-parameter RMO function for both CIGs I used as representative of situations when either strong lateral velocity variations or anisotropy occur. The impact of these improvements in real situation is difficult to predict. More testing and analysis are needed to determine whether the additional computation and code complexity introduced by the addition of a second term to the RMO function are worthy.

The "Orthogonal" RMO function may yields better gradients, but it is also more sensitive with respect to the thickness of the depth-averaging window for the power spectra. This fragility is caused by the location of the extremum of the second term of the "Orthogonal" RMO function in the middle of the angular range. Although the "Orthogonal" function has some theoretical advantages, its lack of robustness make it a less desirable choice.

## REFERENCES

Biondi, B., 2005, Angle-domain common image gathers for anisotropic migration: SEP-Report, **120**, 77–104.

———, 2008, Automatic wave-equation migration velocity analysis: 2008, **134**, 65–77.

———, 2010, Wave-equation migration velocity analysis by residual moveout fitting: SEP-Report, **142**, 25–32.

———, 2011, Migration velocity analysis by one-parameter residual moveout fitting in presence of strong lateral velocity anomalies: SEP-Report, **143**, 59–66.

Biondi, B. and W. W. Symes, 2004, Angle-domain common-image gathers for migration velocity analysis by wavefield-continuation imaging: Geophysics, **69**, 1283–1298.

Siliqi, R., 2009, Structurally coherent wide azimuth residual move out surfaces: SEG Technical Program Expanded Abstracts, **28**, 4039–4043.

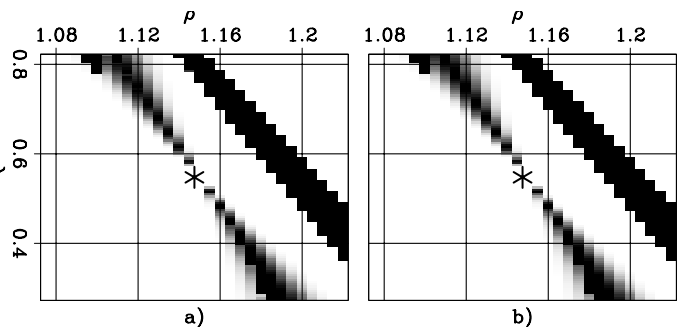


Figure 10: Zooms into the correlation functions shown in Figure 5. [**CR**]

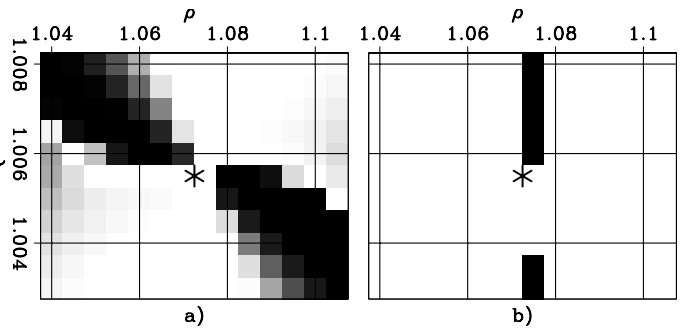


Figure 11: Zooms into the correlation functions shown in Figure 7b and Figure 6b, respectively. [**CR**]

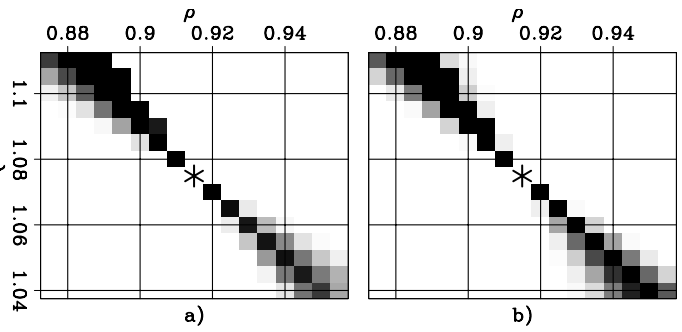


Figure 12: Zooms into the correlation functions shown in Figure 8. [**CR**]

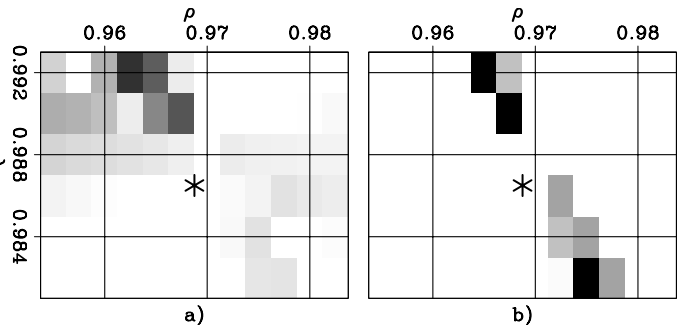


Figure 13: Zooms into the correlation functions shown in Figure 9. [**CR**]

Zhang, Y. and B. Biondi, 2011, Moveout-based wave-equation migration velocity analysis: SEP-Report, **143**, 43–58.